ACS OMEGA

http://pubs.acs.org/journal/acsodf

Article

Eu^{3+}-Doped Electrospun Polyvinylidene Fluoride–Hexafluoropropylene/Graphene Oxide Multilayer Composite Nanofiber for the Fabrication of Flexible Pressure Sensors

Guimao Fu, Qisong Shi,* Yongri Liang,* Yongqing He, Rui Xue, Shifeng He, Yibo Wu, and Rongji Zhou

Cite This: *ACS Omega* 2022, 7, 23521–23531

Read Online

ACCESS | Metrics & More | Article Recommendations | Supporting Information

ABSTRACT: The development of flexible materials with higher piezoelectric properties and electrostrictive response is of great significance in many applications such as wearable functional devices, flexible sensors, and actuators. In this study, we report an efficient fabrication strategy to construct a highly sensitive (0.72 kPa^{-1}), red light-emitting flexible pressure sensor using electrospun Eu^{3+}-doped polyvinylidene fluoride–hexafluoropropylene/graphene oxide composite nanofibers using a layer-by-layer technology. The high β-phase concentration (96.3%) was achieved from the Eu^{3+}-doped P(VDF-HFP)/GO nanofibers, leading to a high piezoelectricity of the composite nanofibers. We observed that a pressure sensor is enabled to generate an output voltage of 4.5 V. Furthermore, Eu^{3+}-doped P(VDF-HFP)/GO composite nanofiber-based pressure sensors can also be used as an actuator as it has a good electrostrictive effect. At the same time, the nanofiber membrane has excellent ferroelectric properties and good fluorescence properties. These results indicate that this material has great application potential in the fields of photoluminescent fabrics, flexible sensors, soft actuators, and energy storage devices.

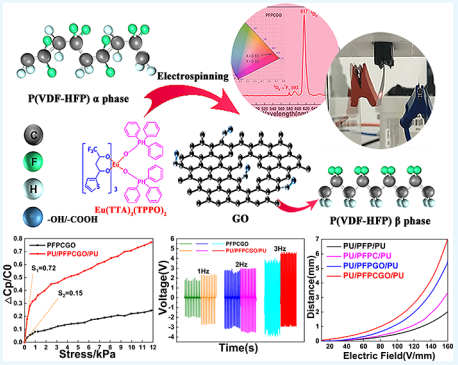

1. INTRODUCTION

In recent years, the application of piezoelectric materials has been expanding. Piezoelectric materials refer to the internal polarization phenomenon when deformation by external force, and the voltage between the two ends of the crystal material, can transform mechanical energy into electrical energy.[1] Electroactive polymers convert electrical energy into mechanical energy with their intrinsic ability, especially under the stimulus of the applied electric field change size or shape (i.e., bending, contraction, or expansion).[2] Organic piezoelectric materials represented by polyvinylidene fluoride (PVDF) and its copolymers have good piezoelectric, ferroelectric, and electrostrictive response properties, which have been widely used in sensors, actuators, energy storage applications, waterproof coatings, and other fields.[3−7]

PVDF and its copolymers mainly have α, β, and γ crystal types. Among them, the β crystal structure with full "TTTT" anticonformation has the largest polarity and exhibits good piezoelectric and electrostrictive properties.[8] Therefore, choosing an appropriate method to increase the content of the β phase is an important research direction to improve the piezoelectric properties of PVDF-based materials, which has important practical application significance. At present, scientists mainly use methods such as high electric field, electrostatic spinning, and polarity induction of nanofillers to increase the content of the β phase.[9−11] The multilayer porous media film prepared using the electrospinning technology has the advantages of easy control, small pore size, and high specific surface area. Under the action of the applied electric field, the polarization effect and the high tensile ratio of the high static electric field in the electrospinning process are similar to uniaxial mechanical drawing, which promotes the increase in the β phase content.[12,13] At the same time, based on the excellent conductivity of conductive fillers, nanofiber membranes are endowed with excellent electrodeformation characteristics under the application of electric field, which opens up the application of piezoelectric nanofiber modified materials for soft actuators.

The doping of rare-earth ions often improves the piezoelectric properties of piezoelectric materials. Eu^{3+} ions were doped in the polyvinylidene fluoride–hexafluoropropylene [P(VDF-HFP)] matrix as fillers to nucleate electrically active β.[14] During electrospinning, the uniform distribution of Eu^{3+} in PVDF nanofibers greatly enhanced the interaction between single Eu^{3+} and adjacent PVDF segments, thus improving the thermal stability of photoluminescence.[15] Among conductive fillers, graphene oxide (GO) is a two-dimensional carbon

Received: April 1, 2022
Accepted: June 2, 2022
Published: June 27, 2022

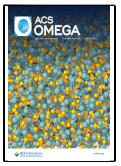

structure with sp^2 hybridization, with high specific surface area, mechanical strength, thermal stability, and a variety of other properties noted. Its surface is bound with a variety of oxygen functional groups, including −COOH and −OH,[16,17] which has a high affinity with surrounding molecules and can promote hydrophilicity and absorption capacity.[18,19] Adding very small amounts of GO with a weight percentage of less than 1% to polymer membranes improves the physicochemical properties of the membranes and generates new functions.[20] The addition of modified particles in the electrospinning process can make the interaction between the polymer and modified particles produce higher charge density, promote the mutually reinforcing crystallization of β, improve its crystallinity, and improve the piezoelectric properties.[21] GO-based composites exhibit significant thermal and mechanical properties attributed to the chemical groups of GO, improving interfacial interactions with other materials/substrates.[22] The mechanical properties of the composites can be optimized by the synergistic effect of multiple fillers, and the piezoelectric properties of the nanocomposite fibers can be enhanced by using multiple fillers.[23]

Multiple conductive fillers were used to improve the electric field distribution or conductive characteristics of the matrix so that the internal charge of the material could be effectively exported to the material surface. Local electric field can be used to make other fillers in the material fully express the effect of electrical coupling.[24] Layered, core-shell, and sandwich structures have been extensively and deeply studied.[25] Sandwich structure polymer nanocomposites can overcome the contradiction between the dielectric constant and breakdown strength, and they have excellent energy storage performance,[26] which contributes to improve the comprehensive performance of composite films. Ahmad et al.[27] found that GO filler had good adsorption performance on the P(VDF-HFP) polymer matrix, and the addition of GO made P(VDF-HFP) PEM have good thermal stability, electrolyte absorption, and morphology. Gao et al.[28] used porous thermoplastic polyurethane (TPU) as a flexible substrate and silver nanowires (AgNWs) as a conductive network system to easily achieve a "sandwich" composite conductive material with high flexibility and low resistance. Rochel and Yalcinkaya[29] prepared PVDF nanofiber multilayers with good hydrophilicity and high mechanical properties through the lamination process, providing a new approach for the design and development of electrospinning filter membranes. Therefore, the development of multifunctional composite piezoelectric materials modified by a foundation structure design is of great significance in many future applications.

In previous studies, we studied the synergic effect of the $BaTiO_3$ system[30] to enhance the function of inorganic fillers and substrate material P(VDF-HFP) and prepared multifunctional nanofiber films with fluorescence, piezoelectric, and ferroelectric properties, which can be used for flexible pressure sensors and energy storage devices. Two-dimensional conductive filler GO has its own unique and excellent performance, which can better improve the mechanical properties and piezoelectric output of the material. Herein, we use two-dimensional conductive filler GO and fluorescent complex Eu$(TTA)_3(TPPO)_2$ to form a double filler system and further explore the influence of double filler components on polymer properties and applications. The β-phase content of the double packing Eu$(TTA)_3(TPPO)_2$/GO system is up to 96.3%, which is used as a sensor with a sensitivity of up to 0.72 kPa^{-1}, 4.5 V ultrahigh output voltage, and 7 mm electroforming variable, and it has good fluorescence characteristics. The multifunctional piezoelectric polymer films developed are of great significance in many application fields such as intelligent wearable devices, flexible sensors, and actuators.

2. EXPERIMENTAL SECTION

2.1. Materials. P(VDF-HFP) (M_w = 400,000) was kindly provided by the Sigma Aldrich (Shanghai) Trading Co., Ltd.; GO (0.92 wt%, diameter: 1 nm, length: 300−1000 nm) was purchased from Shandong OBO New Material Co., Ltd.; thermoplastic polyurethanes (PU, SOFT 45A) were all obtained from BASF (Germany); tetrahydrofuran (THF) and *N*,*N*-dimethylformamide (DMF) were obtained from Shanghai Titan Scientific Co., Ltd. Acetone (Ac) was purchased from Beijing Chemical Works.

2.2. Preparation of Composite Nanofibers. GO aqueous solution (GO: 0.05 wt%) (0.675 g) was dissolved in 4 mL of DMF and 2 mL of Ac mixed solvent, stirred for 10 min, and dispersed by ultrasonication for 30 min to make it evenly dispersed. P(VDF-HFP) particles (1.08 g) were added and stirred at 65 °C for 6 h with magnetic force and dispersed by ultrasonication for 6 h until completely dissolved to obtain 20% (w/v, g/mL) electrostatic spinning precursor solution. Filler fluorescent complex Eu$(TTA)_3(TPPO)_2$ (10 wt%) was added (the preparation method used in our previous report,[30] referred to as C), stirred for 10 min, ultrasonic-dispersed for 30 min, magnetically stirred for 12 h until completely dissolved, and then, 2 mL of the solution was extracted for electrospinning to prepare the nanofiber membrane named PFPCGO. The HD-1311 electrospinning machine of Beijing Yongkang LeYe Technology Development Co., Ltd. is used for electrospinning, and the nanofiber film is collected on the aluminum foil attached to the receiving hub. As a contrast, pure P(VDF-HFP), P(VDF-HFP) spinning solution doped with fluorescent complex C, and P(VDF-HFP) spinning solution doped with GO were prepared at the same time. The nanofiber membranes were prepared by electrostatic spinning and named PFP, PFPC, and PFPGO.

2.3. Fabrication of Sandwiched-Structure Composites. In this work, a sandwiched-structure composite nanofiber membrane was specially designed as the functional layer of the flexible pressure sensor. PU (1.0 g) was dissolved in 2 mL of DMF and 8 mL of THF mixed solution and stirred at room temperature for 5 h until the solution was fully dissolved, which was used to prepare the surface PU nanofiber layer. Through the layer-by-layer spinning method, 2 mL of PU nanofiber layers were spun on both sides of four kinds of PFP, PFPC, PFPGO, and PFPCGO nanofibers, and the four composite nanofibers were successively named PU/PFP/PU, PU/PFPC/PU, PU/PFPGO/PU, and PU/PFPCGO/PU. The specific operation is to electrospun 2 mL of PU spinning solution on aluminum foil paper, continue electrospinning 2 mL of sample liquid under the condition of controlling the same humidity and temperature as possible, and finally electrospun 2 mL of PU spinning solution. The working parameters of electrostatic spinning are as follows: the extrusion rate was set to 1.0 mL/h with a microsyringe pump. The spinning voltage was 18 kV, and the receiving distance was 16 cm. The temperature was maintained at 25 ± 2 °C, and the relative humidity was kept at 40 ± 5%. After drying for 12 h at 25 °C in a vacuum drying oven with a completely volatile solvent and pressing for 5 min at room

https://doi.org/10.1021/acsomega.2c02024
ACS Omega 2022, 7, 23521−23531

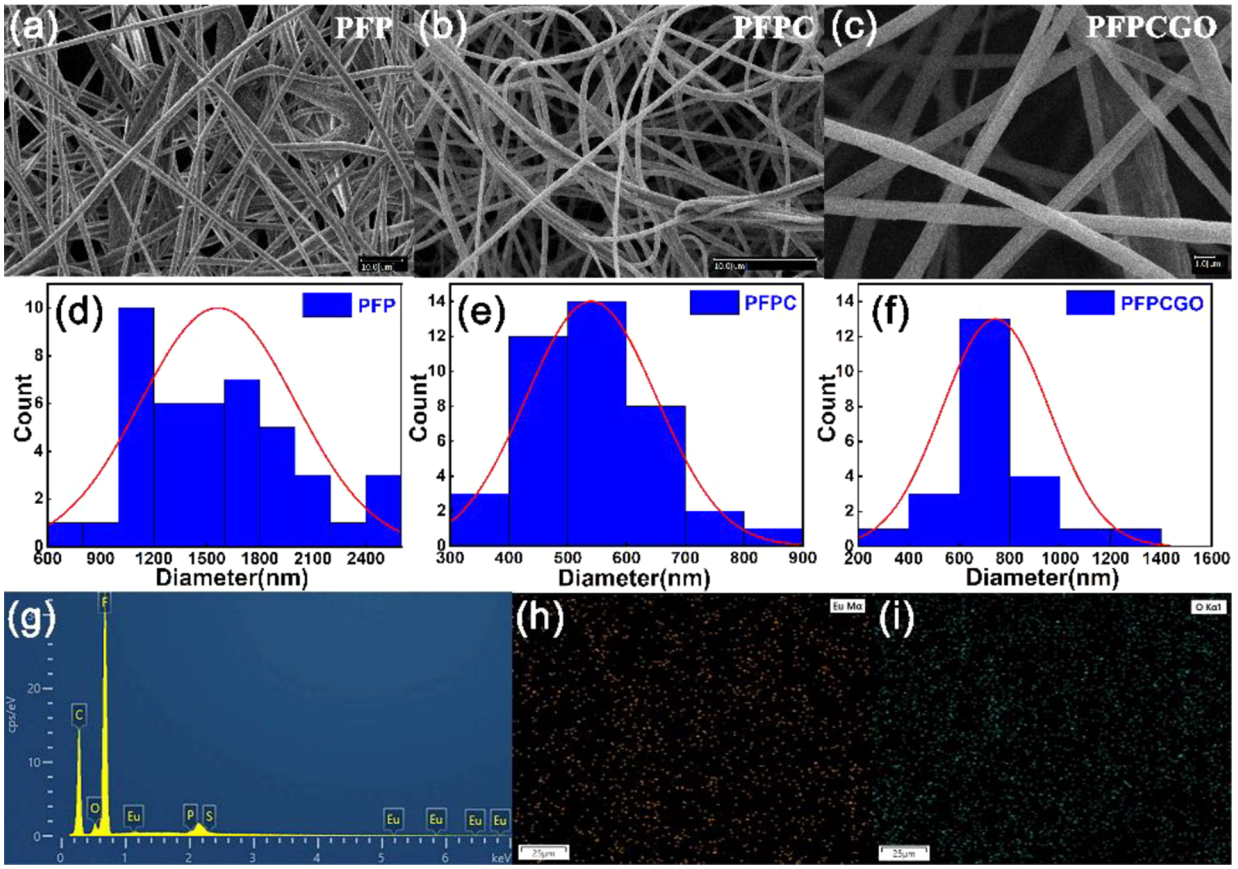

Figure 1. SEM images and diameter distributions of (a) PFP fiber, (b) PFPC nanocomposite fibers, and (c) PFPCGO nanocomposite fibers. Diameter distribution of (d) PFP fiber, (e) PFPC nanocomposite fibers, and (f) PFPCGO nanocomposite fibers. (g) PFPCGO nanofiber element distribution total spectrum. (h) Eu, (i) O element distribution total spectrum.

temperature, the dense PVDF nanofiber membrane was obtained for further experimental characterization.

2.4. Preparation of the Flexible Pressure Sensor. Four kinds of composite nanofiber membranes PU/PFP/PU, PU/PFPC/PU, PU/PFPGO/PU, and PU/PFPCGO/PU were used as the functional layers of the sensor. The composites films were cut into 4 cm × 4 cm, put aluminum foil tape on the two sides of the film, and led out with two thin copper wires.

2.5. Characterization. The surface morphological study of the electrospun composite nanofibers was investigated by a COXEM EM-30PLUSFE-SEM.The diameter of the composite nanofibers was measured using Image J software. Fourier transform infrared (FT-IR) spectra of all the composite nanofibers were recorded using a FTIR-850 FT-IR spectrometer. An FS5 fluorescence spectrometer was used to test the fluorescence of composite nanofibers. The crystalline structures were investigated by X-ray diffraction (XRD). A Setline thermogravimetric analyzer was used to obtain differential scanning calorimetry (DSC) and thermogravimetric curves at a rate of 10 °C/min in the temperature range from room temperature to 800 °C. Atomic force microscopy (AFM) was employed to investigate the surface topography using an AFM machine (MFP-3D, Asylum Research, U.S.A.). Specific probe (AC240TS-R3, Asylum Research) specifications have an elastic coefficient of 2 N/m and a resonance frequency of 70 kHz. The water contact angle (WCA) of the membrane was measured using an optical contact angle and surface tensiometer (SL200KS, KINO USA) using deionized water (5 μL). With the help of a TH2828 Precision LCR Meter Digital Bridge Instrument, the sensitivity of the packaged sensor was tested. A tensile testing machine was used to test the tensile strength of the fiber films, and the polarization−electric field (P−E) hysteresis of the composite nanofibers were studied using a TF2000E ferroelectric analyzer. The electric actuation test was carried out using self-assembled equipment. We used homemade pressure equipment which exerted periodic impact force. A picoammeter (Keithley 6487) and digital oscilloscope (GDS-2102) were used to record piezoelectric current and voltage. The piezoelectric charge coefficient (d_{33}) was measured by ZJ-3AN Piezoelectricity Instrument of Beijing Jingke Zhichuang Technology Co., LTD., China. The sample was prepared by scratch coating with a size of 1 cm × 1 cm and a thickness of about 7 μm. The surface of the sample was sprayed with gold. The sample was polarized for 30 min at 3 kV voltage and stood for 24 h after polarization for testing. All measurements were carried out at room temperature.

3. RESULTS AND DISCUSSION

3.1. Membrane Morphology. Nanofiber membranes were prepared by electrospinning. The scanning electron microscopy (SEM) image and fiber diameter distribution are shown in Figure 1a−c. The figures show randomly oriented fibers without any lumps and an irregular fibrous morphology. Compared with PFP fibers, the diameter of PFPC and PFPCGO nanocomposite fibers decreased from 1000∼2000 nm to 400∼700 nm and 600∼800 nm because of the addition of C and C/GO. This is because the addition of the filler

https://doi.org/10.1021/acsomega.2c02024
ACS Omega 2022, 7, 23521−23531

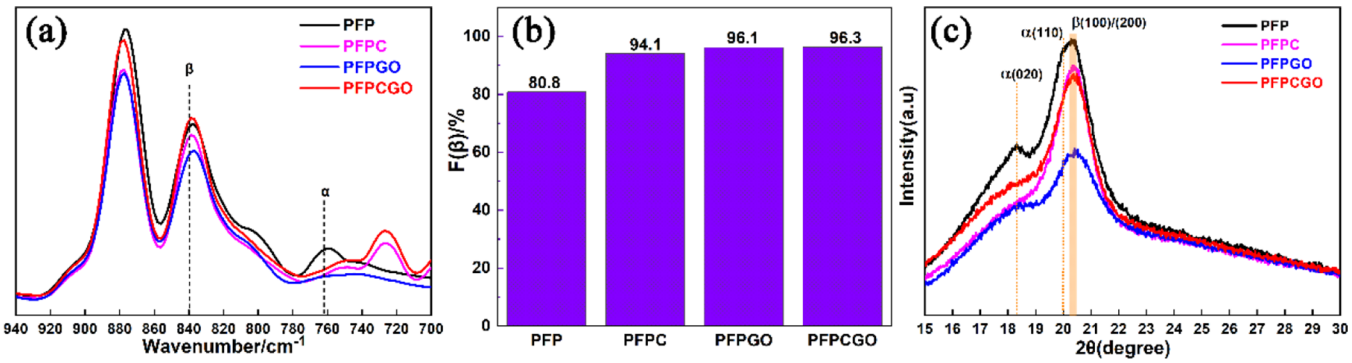

Figure 2. (a) FT-IR spectra for polymer membranes. (b) β crystal content diagram. (c) XRD pattern of the polymer membranes.

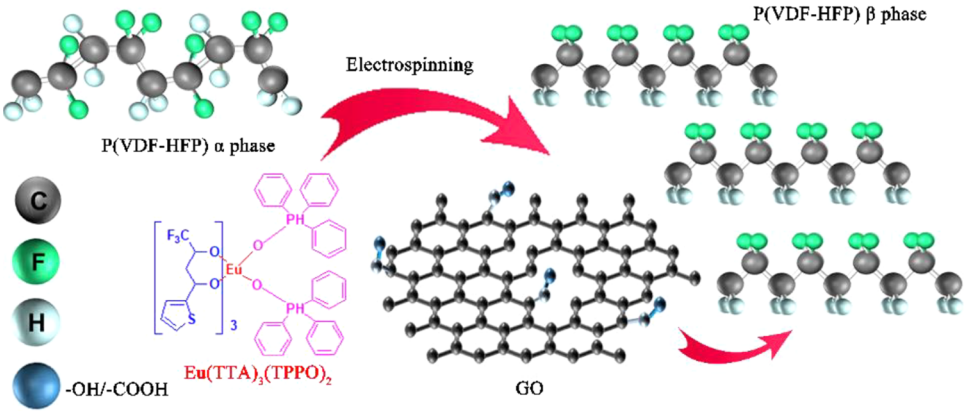

Figure 3. Schematic diagram of increasing the β phase content.

increases the electrical conductivity of electrostatic spinning solution, and the electrostatic repulsion and Coulomb force on Taylor's cone increase during spinning, leading to the reduction of the fiber diameter.[31] There is no obvious granular bulge on the fiber surface, indicating that the doped filler has been well dispersed into the PFP matrix. As can be seen from the energy dispersive X-ray spectroscopy (EDS) in Figure 1d–f, the element composition is complete, and the element is evenly dispersed without aggregation. The uniform dispersion of C with fluorescent properties and conductive GO lays a good foundation for the improvement of P(VDF-HFP) properties.

3.2. Structure and Phase Transformation. The three common conformations of P(VDF-HFP) crystals are α crystal, β crystal, and γ crystal, among which β crystal exhibits piezoelectric properties because of its spontaneous polarization.[32] Different crystal types of P(VDF-HFP) correspond to different FT-IR absorption peaks. The characteristic absorption peaks of the α phase are located at 530, 615, 763, 796, 976, and 1383 cm^{-1}, and the characteristic absorption peaks of the β phase are located at 510, 840, and 1278 cm^{-1}. The peaks at 1234 and 841 cm^{-1} are attributed to the γ-phase and the superimposed β- and γ-phases of P(VDF-HFP), respectively.[33] In order to determine the content of β-phases in the sample, 763 and 840 cm^{-1} were selected to represent the absorption peaks of α and β crystals, respectively. As shown in Figure 2a, it is obvious that the peak height decreases significantly after the doping filler at 763 cm^{-1} because the addition of the filler promotes the transformation of P(VDF-HFP) from the thermally stable α-phase to the metastable β-phase, thus producing more β crystal types. The β crystal content calculated using the Lambert–Beer law is shown in Figure 2b. The β crystal content of the PFP sample is only 80.8%, while the β crystal content of the three samples doped with the filler is 94.1, 96.1, and 96.3%, respectively. It can be seen that the codoping of complex C and GO double packing can promote the increase of the β crystal content, which is 15.5% higher than that of PFP. This result was also confirmed by XRD (Figure 2c) for pure PFP films, and the peaks at 18.4° and 20.0° correspond to the (020) and (110) crystal planes of the P(VDF-HFP) α phase. With the addition of the filler, the characteristic diffraction peak of the α phase almost disappears, and the characteristic diffraction peak of the (100/200) crystal surface of the β phase at 20.4° gradually increases. A special interaction between P(VDF-HFP) and GO further improves the transfer from α to β phases. With the addition of the filler, the intensity of the α phase diffraction peak gradually decreases or even disappears, while the intensity of the β phase diffraction peak gradually increases.

Figure 3 shows the mechanism by which P(VDF-HFP) increases the β phase content. Fluorescence complexes $Eu(TTA)_3(TPPO)_2$ and GO as nucleating agents provide a substrate for the nucleation of P(VDF-HFP) crystals and induce β phase formation through strong interfacial interactions. Because of the high voltage electrostatic field during electrospinning and the high electronegativity of graphene, the H atoms of P(VDF-HFP) tend to be close to the GO surface. The electric field of electrospinning itself, the fluorescence complex, and the local amplified electric field of conductive GO can all generate induced charges, resulting in a stronger Coulomb force, which attracts the P(VDF-HFP) chain to the GO surface to form hydrogen bonds and

https://doi.org/10.1021/acsomega.2c02024
ACS Omega 2022, 7, 23521−23531

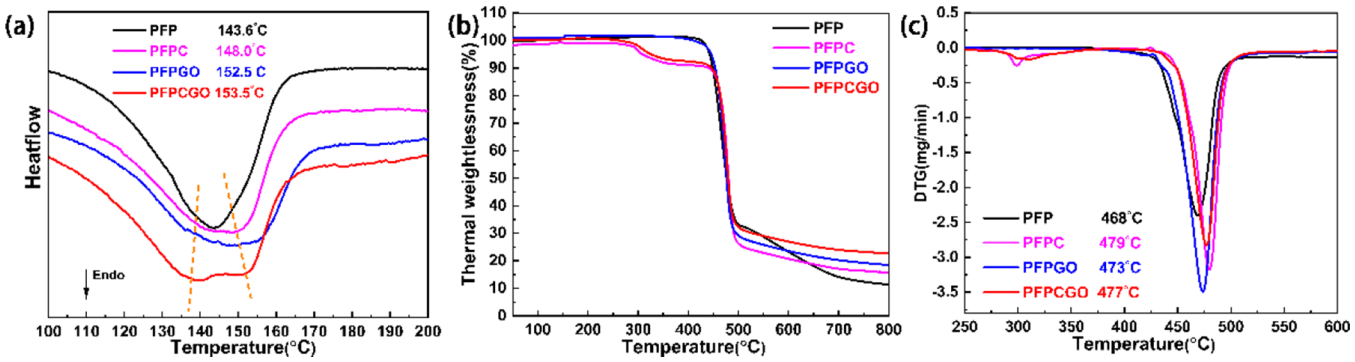

Figure 4. (a) DSC results of polymer membranes. (b) TGA and (c) DTA curves for polymer membranes.

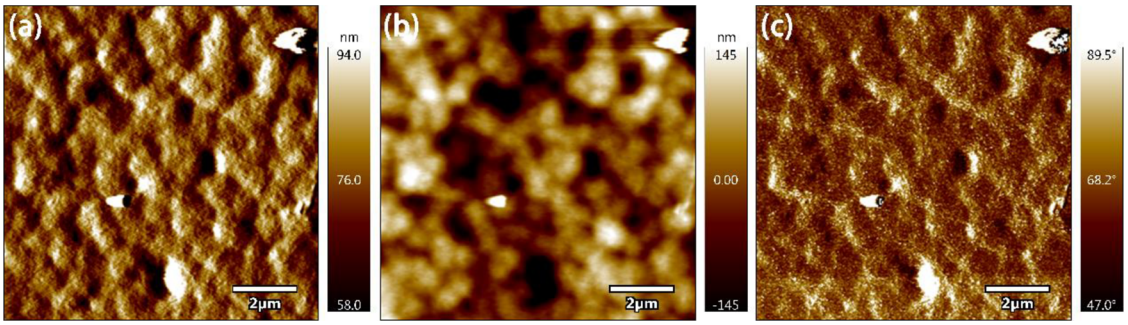

Figure 5. AFM (a) amplitude, (b) height, and (c) phase images of the PFPCGO composite membrane.

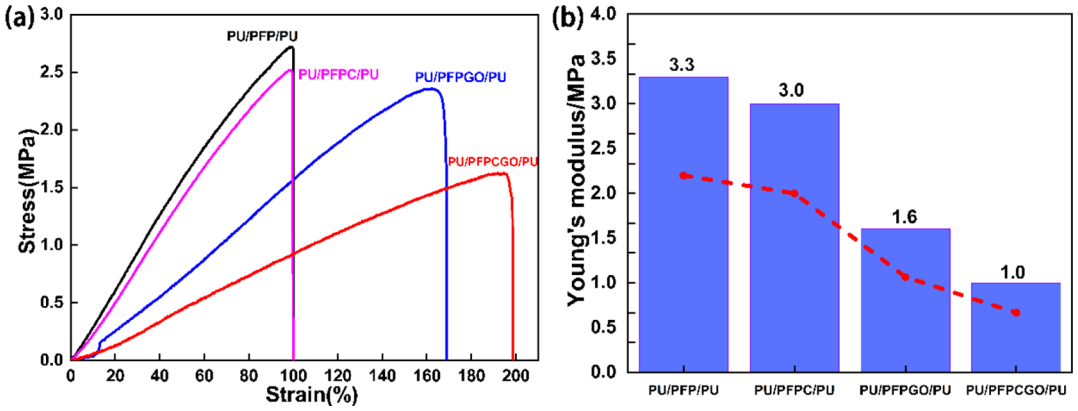

Figure 6. (a) Stress−strain curves and mechanical properties of the nanofibers. (b) Contrast diagram of Young's modulus.

crystallize into the β phase, promoting the increase of the β phase in P(VDF-HFP) composite nanofibers.

DSC thermographs are provided in Figure 4a. The addition of the filler obviously affects the thermal behavior of nanocomposites. For pure PFP, the exothermic peak is 143.6 °C and there is only one large melting peak. With the addition of filler, it is obvious that the melting peak develops into a double wide peak, and the maximum wave peak moves towards high temperature. The melting peak displacement of PFPCGO samples doped with double fillers is the largest, and the exothermic peak is 153.5 °C. The higher melt peak displacement is attributed to the uniform distribution and nucleation of nanoparticles.[34] The GO layer has a good affinity with the polar P(VDF-HFP) chain, resulting in substantial nucleation in the polymer matrix, thus promoting the increase of β crystal content. Figure 4b,c shows the thermogravimetric analysis (TGA) and differential thermal analysis (DTA) curves of the composite. All curves show typical weightlessness at around 470 °C because of the degradation of the polymer chain. Although all samples showed similar degradation characteristics, the percentage of residual mass of the PFPCGO sample was higher than that of other nanocomposites, indicating that the thermal resistance of this particular sample was slightly higher.[35] PFPC and PFPCGO samples have a weightlessness platform corresponding to the weightlessness of the fluorescence complex C at 300 °C, which also proves that the doping of fillers is successful.

PFPCGO spinning solution was scraped and coated with a thickness of about 5 μm. The AFM test was performed. Figure 5 shows the AFM amplitude, height, and phase images of the PFPCGO scratch-coated film. In these images, the brightest areas display the highest point of the membrane surface, and the dark regions represent valley or membrane pores. It can be inferred from AFM images that there are fine particles on the surface of the film, which is due to the diffusion of the nanofillers into the P(VDF-HFP) phase so that the synergistic

https://doi.org/10.1021/acsomega.2c02024
ACS Omega 2022, 7, 23521−23531

effect of the double fillers promotes the increase in the β crystal content.

3.3. Mechanical Property Analysis. The stress−stain curves of electrospun nanofibers are depicted in Figure 6a,b, and the sandwich structure of the PU/PFPCGO/PU nanofiber membrane has a maximum strain of 200%, showing an excellent Young's modulus of 1.0 MPa, but the strain is low, only 1.5 MPa. The maximum strain of the PU/PFPCGO/PU nanofiber membrane of the sandwich structure is doubled than that of pure PU/PFP/PU, while the Young's modulus is reduced by more than three times. It can be seen that doping GO can significantly improve the elongation at break and significantly reduce the Young's modulus of the material, which is far superior to doping complex C. The synergistic effect of the two fillers to enhance the mechanical properties is that the composite nanofibers obtain the maximum elongation at break and the lowest Young's modulus, which makes it more effective in the application of flexible pressure sensors.

3.4. Ferroelectric Performance Analysis. Figure 7 describes the ferroelectric properties of nanofiber samples. It

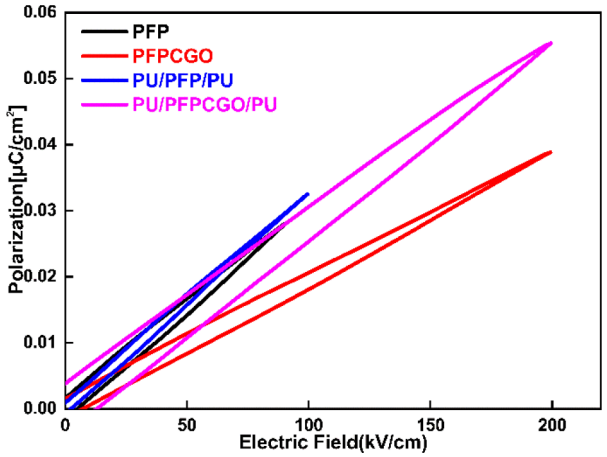

Figure 7. Polarization−electric field (P−E) hysteresis of composite nanofibers.

can be seen that the addition of the filler and sandwich structure design obviously enhances the ferroelectric properties of the material. Saturation polarization (P_s) was significantly enhanced, in which $P_{s\text{-PFP}}$: 0.028 μC/cm^2, $P_{s\text{-PU/PFP/PU}}$: 0.033 μC/cm^2, $P_{s\text{-PFPCGO}}$: 0.039 μC/cm^2, and $P_{s\text{-PU/PFPCGO/PU}}$: 0.055 μC/cm^2. The remnant polarization (P_r) of 4.0 × 10^{-3} μC/cm^2 is obtained for PU/PFPCGO/PU, which is higher than that of PFPCGO (a negligible value of 1.7 × 10^{-3} μC/cm^2), indicating that the sandwich structure can improve the ferroelectric properties of the material efficiently. Although the sandwich structure conductive filler system can also improve the ferroelectric properties of materials, the residual polarization and saturation polarization values are far less than those of the inorganic filler system [Eu(TTA)$_3$(TPPO)$_2$/BaTiO$_3$].

3.5. Surface WCA of Electrospun Membranes. The surface hydrophobicity of different nanofibrous layers was evaluated using dynamic WCA measurements [Figure 8a−c]. The WCA over 90° means that nanofibers surface is hydrophobic in nature. PU has a hydrophobic surface with a WCA of 117°. The WCA of PFPCGO nanofiber membrane was 122°. We found that the sandwich structure of the PU/PFPCGO/PU nanofiber membrane WCA was 123° close to

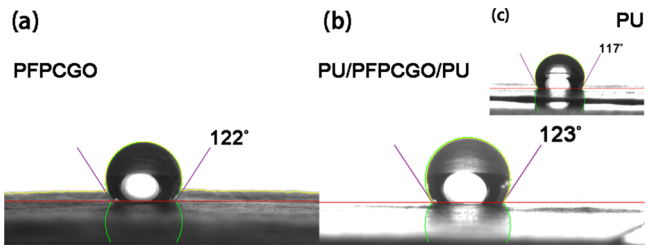

Figure 8. WCA images of (a) PFPCGO, (b) PU/PFPCGO/PU, and (c) PU composite nanofibers.

the PFPCGO nanofiber membrane, which maintained the surface hydrophobicity of the material. Therefore, the obtained PU/PFPCGO/PU film exhibited great hydrophobicity, making it a promising candidate to be fabricated into a flexible press sensor and some intelligent wearable devices.

3.6. Fluorescence Properties of Electrospun Membranes. Figure 9 shows the fluorescence emission spectrum of

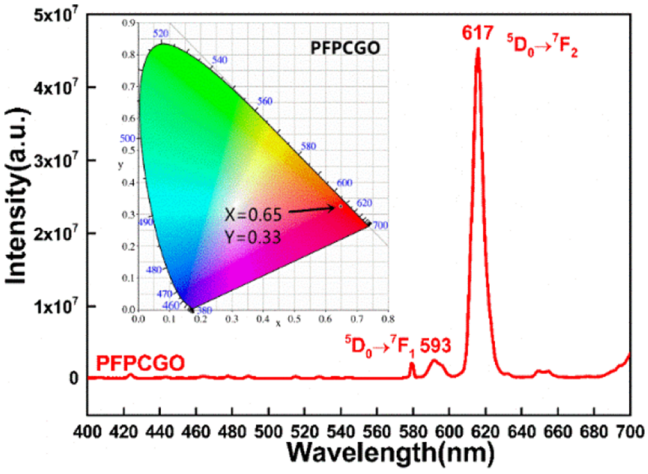

Figure 9. Fluorescence spectra of PFPCGO.

the PFPCGO nanofiber membrane. The emission peak is strong at 593 and 617 nm, corresponding to the $^5D_0 \rightarrow {}^7F_1$ and $^5D_0 \rightarrow {}^7F_2$ electron transitions of Eu^{3+}. The emission peak is the strongest at 617 nm, which is the characteristic peak of Eu^{3+}. The calculated peak points (x = 0.65, y = 0.33) correspond to red emission in CIE color coordinates, which provides a basis for the realization of flexible pressure sensors that can be fluorescently labeled.

3.7. Sensitivity of the Flexible Pressure Sensor. The flexible pressure sensor is prepared using the method explained in Section 2.4. Our flexible pressure sensor has a positive capacitance change and can show a capacitance curve that increases with the application of pressure when applied. When the external pressure, the top and bottom when the distance between the electrodes is reduced, the internal nanofibers in thickness can be reduced, nanofibers the increase of contact area, and separation to shorten the distance between electrode lead to pressure sensor capacitance increased significantly when compressed, so within the scope of the low pressure with high stress sensitivity. The flexible pressure sensor based on the piezoelectric sandwich nanofiber membrane acts as a capacitor. Therefore, when the piezoelectric voltage is generated under applied stress, the induced charge accumulates on the electrode surface, which will cause the change of the capacitance of the

https://doi.org/10.1021/acsomega.2c02024
ACS Omega 2022, 7, 23521−23531

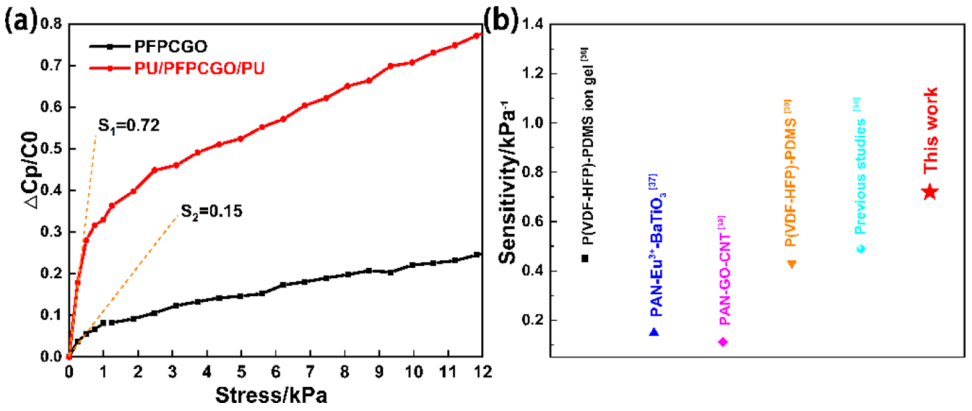

Figure 10. (a) Comparison of the sensitivity of PFPCGO and PU/PFPCGO/PU sensors. (b) Comparison of the sensitivity of sensors in this study and the reported literature.

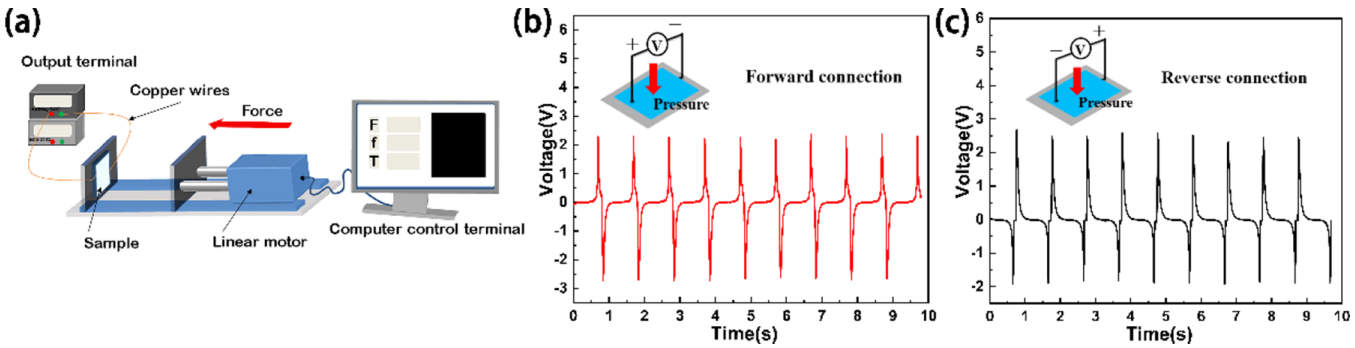

Figure 11. (a) Schematic diagram of the piezoelectric response measurement system. Output voltage of (b) the forward connection and (c) the reverse connection.

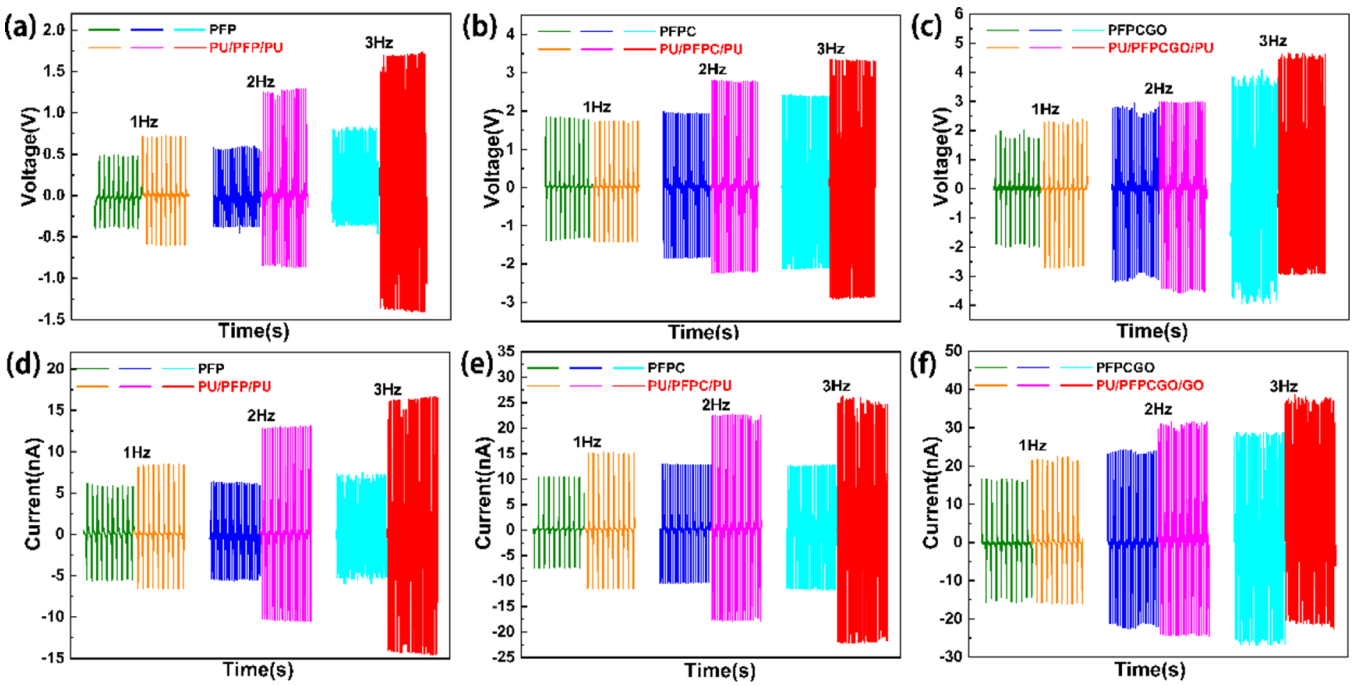

Figure 12. Piezoelectric output (a–c) voltage and (d–f) current of the nanocomposites under different frequencies (1~3 Hz).

device. The sensitivity of the device can be measured by the change in the capacitance value with the change in pressure. As shown in Figure 10a, when the pressure is less than 1 kPa, it is obvious that the PU/PFPCGO/PU film has an excellent sensitivity of 0.72 kPa^{-1}, about 4.8 times that of the PFPCGO sample (0.15 kPa^{-1}), and much higher than that reported in some literature.[36−39] [Figure 10b]. With increasing pressure, sensitivity decreases and tends to equilibrium. Therefore, in the low-pressure range, the pressure sensitivity is more

https://doi.org/10.1021/acsomega.2c02024
ACS Omega 2022, 7, 23521−23531

Table 1. Compared with Other Reported Piezoelectric Outputs

materials	area [cm^2]	frequency [Hz]	force [N]	d_{33} [pC/N]	voltage [V]	current [nA]	ref.
P(VDF-HFP)-Co-ZnO		50	2.5		2.8		34
PVDF-GO-BTO	1	2	10	38	2.5	10.5	42
P(VDF-HFP)/MWCNT			15		0.62		43
PVDF-GO/graphene	35			24	2	600	44
PVDF-GO	4	8	12	12.25	2.1		45
PVDF-rGO	20	5			4.38		46
PVDF-GO	35	2	0.49	0.65	0.08	70	47
P(VDF-HFP)-GO-Eu^{3+}	**16**	**3**	**20**	**4**	**4.5**	**35**	**this work**

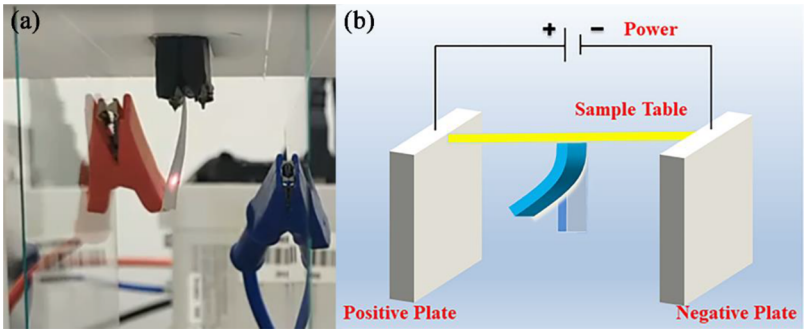

Figure 13. (a) Electrostrictive test device and (b) schematic diagram.

excellent, making it useful as an electronic skin to detect small vibrations such as pulse and heart rate.[39]

3.8. Piezoelectric Studies of the Flexible Pressure Sensor. Figure 11a shows the schematic diagram of the piezoelectric response measurement system. The computer control terminal can ensure that the linear motor can provide a certain frequency and a certain value of pressure. Test results are displayed and recorded on the output terminal. We conducted a polarity test by reversing electrode connection, as shown in Figure 11b,c, the output voltage is basically the same, but the opposite polarity, which confirmed the arrangement of dipole. It also shows that when the sensor is subjected to external stress changes, piezoelectric potential will be generated due to the existing polarization changes, that is, the measured output electrical signal is generated by the piezoelectric effect.

It is observed that the piezoelectric property of polymer nanocomposites strongly depends on the crystalline structure of the polymer, as well as on the electroactive polar phase formation in the nanocomposite.[35] In order to study the piezoelectric properties of the prepared flexible pressure sensor, the output voltage and current were tested at the same pressure of 20 N and different frequencies (Figure 12). The output voltage is not only dependent on the β crystal content but also depends on the effect of the vibration frequency applied to the sample.[40] It can be seen from the figure that the output voltage and current are proportional to the frequency, which means that the sensor can have good response under different environmental changes. With the addition of the filler, when the test condition is 3 Hz, the voltage output of PFP, PFPC, and PFPCGO is 0.8, 2.2, and 3.8 V, respectively. The voltage output of PU/PFP/PU, PU/PFPC/PU, and PU/PFPCGO/PU with the sandwich structure is 1.7, 3.2, and 4.5 V, respectively. The output of the sandwich structure is better than that of the single layer structure, and the addition of the filler is better than that of pure P(VDF-HFP). By providing more nucleating sites, GO increased the β phase proportion and therefore enhanced the electrical properties of PVDF.[41] The study found that at 3 Hz, the piezoelectric output of the PU/PFPCGO/PU double-packing system with the sandwich structure was the highest, with an output voltage of about 4.5 V and an output current of about 35 nA, which were far better than those reported in the literature, as shown in Table 1. In order to better demonstrate the piezoelectric properties of the material, the piezoelectric charge coefficient (d_{33}) of the PFPCGO spinning solution is 4 pC/N after scraping and coating the film, which proves that the material has certain piezoelectric properties. There is still a certain gap with some reported data in Table 1. The reason should be that the electrode prepared by nanofiber film will always be broken down, and the scraping process is adopted. Therefore, the device can be used for pressure detection, signal monitoring, and electronic skin sensing.

3.9. Electrostrictive Test. The electrostrictive test device and schematic diagram is shown in Figure 13. The sample was clamped with a clamp to expose it for 20 mm, and the laser table was adjusted so that the laser hits 5 mm upward at the bottom of the sample, that is, the displacement (D) at 15 mm away from the fixed position. The positive and negative power supplies are connected to the conductive glass, and the electric field spacing is 40 mm. Without prepolarization, the electrostrictive test was carried out. The electrostrictive test is to gradually increase the voltage from 400 to 6400 V and increase the interval by 50 V/0.01 s each time. The electrostrictive test cycle test is to momentarily apply a voltage of 4500 V, maintain for 20 s, disconnect for 20 s, and cycle 10 times. The cycle test is to continue after the electrostrictive test of the same sample. The nanofiber layer was spun on the surface of aluminum foil using the layer spinning method. The difference is that electrospun 6 mL (expanded by 3 times) of PU/PFP/PU, PU/PFPC/PU, PU/PFPGO/PU, and PU/PFPCGO/PU precursors are electrically driven samples. The PU nanofiber layer (2 mL) was electrospun on both sides of the surface, and the

https://doi.org/10.1021/acsomega.2c02024
ACS Omega 2022, 7, 23521−23531

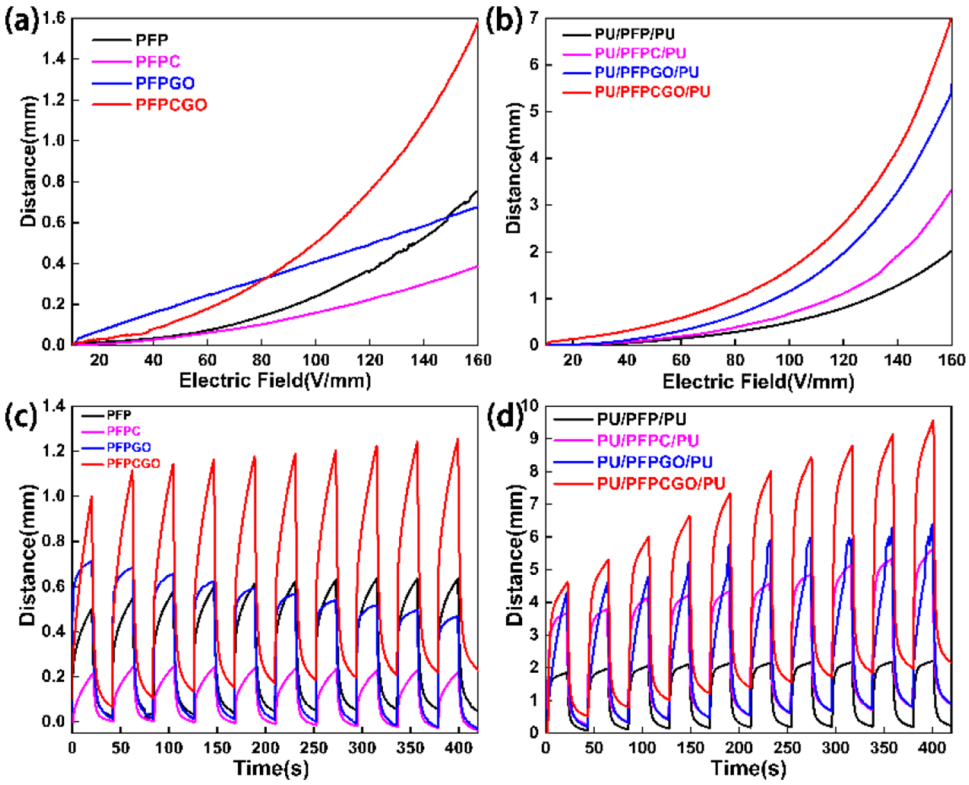

Figure 14. Response performance of samples (40 mm long, 5 mm wide, and 0.2 mm thick) to high voltage electric field. Bending displacements (D) of (a) monolayer and (b) sandwich structures. Bending displacement curves of (c) monolayer and (d) sandwich structures under cyclic electric field.

sample was cut into 40 mm × 5 mm with a thickness of 0.2 ± 0.05 mm. The test results are shown in Figure 13.

It can be seen from Figure 14 and the Supporting Information Videos 1 and 2 that the sample of the electrostatic spinning nanofiber film with a sandwich structure deforms under the action of the applied electric field, and the deformation is restored after the electric field is removed.[48] In the absence of any applied electric field, the dipoles in the nanofibers are randomly oriented. When an electric field is applied, the dipoles are oriented according to the electric field, so the sample will shrink.[49] The maximum deformation of sample PU/PFPCGO/PU is ∼7 mm, which is about 4.4 times the deformation of sample PFPCGO (∼1.6 mm) and 8.8 times that of PFP (∼0.8 mm). It can be seen from the curve slope that the response of the double filler system is also relatively fast, and the slope increases gradually with the increase in the electric field, which indicates that the response and deformation increase sharply with the increase in the electric field. It can be seen that the double filler system[50] and the sandwich structure can more effectively promote the driving performance of the film. Figure 14b shows the bending displacement curve of the sample under the cyclic electric field; it can be seen that the deformation increases rapidly at the beginning of applying the fixed electric field, and the deformation increases slowly with the change in time. After removing the electric field, the deformation decreases sharply, but it cannot return to the initial position, where certain deflection is maintained, and the deflection begins to increase with the increase in the number of cycles. The double filler system and the sandwich structure of the nanofiber membrane have a more obvious electric deformation effect.

4. CONCLUSIONS

In conclusion, the mechanical properties of the conductive filler system are obviously better than those of the inorganic filler system, and Young's modulus is greatly reduced. Although the sandwich structure conductive filler system can also improve the ferroelectric properties of materials, the residual polarization and saturation polarization values are far less than those of the inorganic filler system. The synergism of the conductive filler and the fluorescence complex reduced the fiber diameter and promoted the transformation of α to β phase in P(VDF-HFP) nanofibers, and the β phase content increased by 96.3%. In terms of sensor performance, the sandwich structure sensor is far superior to the monolayer, with a sensitivity of up to 0.72 kPa^{-1}, an ultrahigh output voltage of 4.5 V, and an electroforming variable of 7 mm. The stability, repeatability, durability, and applicability on practical fields of this multilayer nanofiber composites are also very important, which is the direction we need to further study in the future. The sandwich structure nanofiber membrane prepared has good hydrophobicity and certain fluorescence properties. The flexible sensor based on the electrostatic spinning sandwich structure double-packing system nanocomposite fiber has ultrahigh and low voltage sensitivity, high piezoelectric output, good fluorescence function, excellent mechanical properties, and so on, which has great application potential in multifunctional flexible sensors, actuators, and other fields.

https://doi.org/10.1021/acsomega.2c02024
ACS Omega 2022, 7, 23521−23531

■ ASSOCIATED CONTENT

Supporting Information

The Supporting Information is available free of charge at https://pubs.acs.org/doi/10.1021/acsomega.2c02024.

Electrostrictive: the application and maintenance of electric fields (MP4)

Electrostrictive: the maintenance and cancellation of the electric field (MP4)

■ AUTHOR INFORMATION

Corresponding Authors

Qisong Shi − *Beijing Key Lab of Special Elastomeric Composite Materials, College of New Materials and Chemical Engineering, Beijing Institute of Petrochemical Technology, Beijing 102617, China;* orcid.org/0000-0001-8118-5980; Email: shiqisong@bipt.edu.cn

Yongri Liang − *State Key Lab of Metastable Materials Science and Technology, School of Materials Science and Engineering, Yanshan University, Hebei 066012, China;* orcid.org/0000-0003-3576-613X; Email: liangyr@ysu.edu.cn

Authors

Guimao Fu − *Beijing Key Lab of Special Elastomeric Composite Materials, College of New Materials and Chemical Engineering, Beijing Institute of Petrochemical Technology, Beijing 102617, China*

Yongqing He − *Beijing Key Lab of Special Elastomeric Composite Materials, College of New Materials and Chemical Engineering, Beijing Institute of Petrochemical Technology, Beijing 102617, China*

Rui Xue − *Beijing Key Lab of Special Elastomeric Composite Materials, College of New Materials and Chemical Engineering, Beijing Institute of Petrochemical Technology, Beijing 102617, China*

Shifeng He − *Beijing Key Lab of Special Elastomeric Composite Materials, College of New Materials and Chemical Engineering, Beijing Institute of Petrochemical Technology, Beijing 102617, China*

Yibo Wu − *Beijing Key Lab of Special Elastomeric Composite Materials, College of New Materials and Chemical Engineering, Beijing Institute of Petrochemical Technology, Beijing 102617, China;* orcid.org/0000-0002-3739-4643

Rongji Zhou − *Beijing Key Lab of Special Elastomeric Composite Materials, College of New Materials and Chemical Engineering, Beijing Institute of Petrochemical Technology, Beijing 102617, China*

Complete contact information is available at: https://pubs.acs.org/10.1021/acsomega.2c02024

Author Contributions

All authors contributed to the writing of this manuscript and gave their approval for the final version.

Notes

The authors declare no competing financial interest.

■ ACKNOWLEDGMENTS

This study was supported by the National Natural Science Foundation of China (No. 52073033), the fund of the Beijing Municipal Education Commission, China (No. 22019821001). Beijing excellent talents training fund (No. Z2019-042). Open Research Fund from Zhejiang Collaborative Innovation Center for High Value Utilization of byproducts from Ethylene Project (Ningbo Polytechnic College) in 2021−2022 (No. NZXT202102), College Student Research and Career-creation Program of Beijing City, China (No. 2022 J00044), and Yanshan Scholars' Scientific Research Start-up Funding from Yanshan University, China.

■ REFERENCES

(1) Chen, C.; Bai, Z.; Cao, Y.; Dong, M.; Jiang, K.; Zhou, Y.; Tao, Y.; Gu, S.; Xu, J.; Yin, X.; Xu, W. Enhanced piezoelectric performance of $BiCl_3$/PVDF nanofibers-based nanogenerators. *Compos. Sci. Technol.* **2020**, *192*, No. 108100.

(2) D'Anniballe, R.; Zucchelli, A.; Carloni, R. Towards Poly (vinylidene fluoride-trifluoroethylene-chlorotrifluoroethylene)-based soft actuators: Films and electrospun aligned nanofiber mats. *Nanomaterials* **2021**, *11*, 172.

(3) Ponnan, S.; Schmidt, T. W.; Li, T.; Gunasekaran, H. B.; Ke, X.; Huang, Y.; Wu, L. Electrospun Polyvinylidene Fluoride−Magnesio-chromite Nanofiber-Based Piezoelectric Nanogenerator for Energy Harvesting Applications. *ACS Appl. Polym. Mater.* **2021**, *3*, 4879−4888.

(4) Pratihar, S.; Patra, A.; Sasmal, A.; Medda, S. K.; Sen, S. Enhanced dielectric, ferroelectric, energy storage and mechanical energy harvesting performance of ZnO−PVDF composites induced by MWCNTs as an additive third phase. *Soft Matter* **2021**, *17*, 8483−8495.

(5) Hu, Y.; Wang, Z. L. Recent progress in piezoelectric nanogenerators as a sustainable power source in self-powered systems and active sensors. *Nano Energy* **2015**, *14*, 3−14.

(6) Wu, H.; Huang, Y.; Xu, F.; Duan, Y.; Yin, Z. Energy harvesters for wearable and stretchable electronics: from flexibility to stretchability. *Adv. Mater.* **2016**, *28*, 9881−9919.

(7) Subrahmanya, T. M.; Arshad, A. B.; Lin, P. T.; Widakdo, J.; Makari, H. K.; Austria, H. F. M.; Hung, W. S. A review of recent progress in polymeric electrospun nanofiber membranes in addressing safe water global issues. *RSC Adv.* **2021**, *11*, 9638−9663.

(8) Cai, J.; Hu, N.; Wu, L.; Liu, Y.; Li, Y.; Ning, H.; Lin, L. Preparing carbon black/graphene/PVDF-HFP hybrid composite films of high piezoelectricity for energy harvesting technology. *Composites, Part A* **2019**, *121*, 223−231.

(9) Garain, S.; Jana, S.; Sinha, T. K.; Mandal, D. Design of In Situ Poled Ce^{3+}-Doped Electrospun PVDF/Graphene Composite Nanofibers for Fabrication of Nanopressure Sensor and Ultrasensitive Acoustic Nanogenerator. *ACS Appl. Mater. Interfaces* **2016**, *8*, 4532−4540.

(10) Priya, L.; Jog, J. P. Poly(vinylidene fluoride)/clay nanocomposites prepared by melt intercalation: Crystallization and dynamic mechanical behavior studies. *J. Polym. Sci., Part B: Polym. Phys.* **2002**, *40*, 1682−1689.

(11) Khalifa, M.; Mahendran, A.; Anandhan, S. Probing the synergism of halloysite nanotubes and electrospinning on crystallinity, polymorphism and piezoelectric performance of poly (vinylidene fluoride). *RSC Adv.* **2016**, *6*, 114052−114060.

(12) Xue, J.; Wu, T.; Dai, Y.; Xia, Y. Electrospinning and electrospun nanofibers: Methods, materials, and applications. *Chem. Rev.* **2019**, *119*, 5298−5415.

(13) Zhang, Z.; Wang, X.; Tan, S.; Wang, Q. Superior electrostrictive strain achieved under low electric fields in relaxor ferroelectric polymers. *J. Mater. Chem. A* **2019**, *7*, 5201−5208.

(14) Adhikary, P.; Garain, S.; Ram, S.; Mandal, D. Flexible hybrid Eu^{3+} doped P(VDF-HFP) nanocomposite film possess hypersensitive electronic transitions and piezoelectric throughput. *J. Polym. Sci., Part B: Polym. Phys.* **2016**, *54*, 2335−2345.

(15) Zhang, X.; Wen, S.; Hu, S.; Chen, Q.; Fong, H.; Zhang, L.; Liu, L. Luminescence properties of Eu (III) complex/polyvinylpyrrolidone electrospun composite nanofibers. *J. Phys. Chem. C* **2010**, *114*, 3898−3903.

(16) Wilczewski, S.; Skorczewska, K.; Tomaszewska, J.; Lewandowski, K.; Szulc, J.; Runka, T. Manufacturing homogenous

PVC/graphene nanocomposites using a novel dispersion agent. *Polym. Test.* **2020**, *91*, No. 106868.
(17) Wang, L.; Wei, X.; Wang, G.; Zhao, S.; Cui, J.; Gao, A.; Yan, Y. A facile and industrially feasible one-pot approach to prepare graphene-decorated PVC particles and their application in multifunctional PVC/graphene composites with segregated structure. *Composites, Part B* **2020**, *185*, No. 107775.
(18) Zhang, Y.; Wang, Y.; Cao, X.; Xue, J.; Zhang, Q.; Tian, J.; Zheng, X. Effect of carboxyl and hydroxyl groups on adsorptive polysaccharide fouling: A comparative study based on PVDF and graphene oxide (GO) modified PVDF surfaces. *J. Membr. Sci.* **2020**, *595*, No. 117514.
(19) Abd El-Kader, M. F. H.; Awwad, N. S.; Ibrahium, H. A.; Ahmed, M. K. Graphene oxide fillers through polymeric blends of PVC/PVDF using laser ablation technique: electrical, antibacterial, and thermal stability. *J. Mater. Res. Technol.* **2021**, *13*, 1878−1886.
(20) Wang, X.; Zhao, Y.; Tian, E.; Li, J.; Ren, Y. Graphene oxide-based polymeric membranes for water treatment. *Adv. Mater. Interfaces* **2018**, *5*, No. 1701427.
(21) Karan, S. K.; Bera, R.; Paria, S.; Das, A. K.; Maiti, S.; Maitra, A.; Khatua, B. B. An Approach to Design Highly Durable Piezoelectric Nanogenerator Based on Self-Poled PVDF/AlO-rGO Flexible Nanocomposite with High Power Density and Energy Conversion Efficiency. *Adv. Energy Mater.* **2016**, *6*, No. 1601016.
(22) Valentini, L.; Rescignano, N.; Puglia, D.; Cardinali, M.; Kenny, J. Preparation of alginate/graphene oxide hybrid films and their integration in triboelectric generators. *Eur. J. Inorg. Chem.* **2015**, *2015*, 1192−1197.
(23) Ponnamma, D.; Parangusan, H.; Tanvir, A.; AlMa'adeed, M. A. A. Smart and robust electrospun fabrics of piezoelectric polymer nanocomposite for self-powering electronic textiles. *Mater. Des.* **2019**, *184*, No. 108176.
(24) Zhang, S.; An, Q. Progress on the Design and Fabrication of High Performance Piezoelectric Flexible Materials Based on Polyvinylidene Fluoride. *Chem. J. Chin. Univ.* **2021**, *42*, 1114−1145.
(25) Zhao, S.; Yan, L.; Tian, X.; Liu, Y.; Chen, C.; Li, Y.; Qin, Y. Flexible design of gradient multilayer nanofilms coated on carbon nanofibers by atomic layer deposition for enhanced microwave absorption performance. *Nano Res.* **2018**, *11*, 530−541.
(26) Wang, Y.; Wang, L.; Yuan, Q.; Chen, J.; Niu, Y.; Xu, X.; Wang, H. Ultrahigh energy density and greatly enhanced discharged efficiency of sandwich-structured polymer nanocomposites with optimized spatial organization. *Nano Energy* **2018**, *44*, 364−370.
(27) Ahmad, A. L.; Farooqui, U. R.; Hamid, N. A. Effect of graphene oxide (GO) on Poly(vinylidene fluoride-hexafluoropropylene) (PVDF-HFP) polymer electrolyte membrane. *Polymer* **2018**, *142*, 330−336.
(28) Gao, Q.; Kopera, B. A.; Zhu, J.; Liao, X.; Gao, C.; Retsch, M.; Greiner, A. Breathable and flexible polymer membranes with mechanoresponsive electric resistance. *Adv. Funct. Mater.* **2020**, *30*, No. 1907555.
(29) Roche, R.; Yalcinkaya, F. Incorporation of PVDF nanofibre multilayers into functional structure for filtration applications. *Nanomaterials* **2018**, *8*, 771.
(30) Fu, G.; Shi, Q.; He, Y.; Xie, L.; Liang, Y. Electroactive and photoluminescence of electrospun P(VDF-HFP) composite nanofibers with Eu^{3+} complex and $BaTiO_3$ nanoparticles. *Polymer* **2022**, *240*, No. 124496.
(31) Azimi, B.; Milazzo, M.; Lazzeri, A.; Berrettini, S.; Uddin, M. J.; Qin, Z.; Danti, S. Electrospinning piezoelectric fibers for biocompatible devices. *Adv. Healthcare Mater.* **2020**, *9*, No. 1901287.
(32) Tian, G.; Deng, W.; Gao, Y.; Xiong, D.; Yan, C.; He, X.; Yang, W. Rich lamellar crystal bak-lava-structured PZT/PVDF piezoelectric sensor toward individual table tennis training. *Nano Energy* **2019**, *59*, 574−581.
(33) Ince-Gunduz, B. S.; Alpern, R.; Amare, D.; Crawford, J.; Dolan, B.; Jones, S.; Cebe, P. Impact of Nanosilicates on Poly(Vinylidene Fluoride) Crystal Polymorphism: Part 1. Melt-Crystallization at High Supercooling. *Polymer* **2010**, *51*, 1485−1493.
(34) Liang, J.; Luo, J.; Zhang, J.; Xiong, Y.; Tan, S. Constructing a High-Density Thermally Conductive Network through Electrospinning−Hot-Pressing of BN@ PDA/GO/PVDF Composites. *ACS Appl. Polym. Mater.* **2022**, *4*, 2414−2422.
(35) Ponnamma, D.; Aljarod, O.; Parangusan, H.; Al-Maadeed, M. A. A. Electrospun nanofibers of PVDF-HFP composites containing magnetic nickel ferrite for energy harvesting application. *Mater. Chem. Phys.* **2020**, *239*, No. 122257.
(36) Lin, M. F.; Xiong, J.; Wang, J.; Parida, K.; Lee, P. S. Core-Shell nanofiber mats for tactile pressure semmcnsor and nanogenerator applications. *Nano Energy* **2018**, *44*, 248−255.
(37) He, Y.; Fu, G.; He, D.; Shi, Q.; Chen, Y. Fabrication and characterizations of Eu^{3+} doped PAN/$BaTiO_3$ electrospun piezoelectric composite fibers. *Mater. Lett.* **2022**, *314*, No. 131888.
(38) Ma, Y.; Ouyang, J.; Raza, T.; Li, P.; Jian, A.; Li, Z.; Tao, G. Flexible all-textile dual tactile-tension sensors for monitoring athletic motion during taekwondo. *Nano Energy* **2021**, *85*, No. 105941.
(39) Luo, Z.; Chen, J.; Zhu, Z.; Li, L.; Su, Y.; Tang, W.; Li, H. High-Resolution and High-Sensitivity Flexible Capacitive Pressure Sensors Enhanced by a Transferable Electrode Array and a Micropillar−PVDF Film. *ACS Appl. Mater. Interfaces* **2021**, *13*, 7635−7649.
(40) Ponnamma, D.; Erturk, A.; Parangusan, H.; Deshmukh, K.; Ahamed, M. B.; Al-Maadeed, A. A. M. Stretchable quaternary phasic PVDF-HFP nanocomposite films containing graphene-titania-$SrTiO_3$ for mechanical energy harvesting. *Energy Mater.* **2018**, *1*, 55−65.
(41) Cherumannil Karumuthil, S.; Prabha Rajeev, S.; Valiyaneerilakkal, U.; Athiyanathil, S.; Varghese, S. Electrospun poly(vinylidene fluoride-trifluoroethylene)-based polymer nanocomposite fibers for piezoelectric nanogenerators. *ACS Appl. Mater. Interfaces* **2019**, *11*, 40180−40188.
(42) Zhu, M.; Lou, M.; Abdalla, I.; Yu, J.; Li, Z.; Ding, B. Highly shape adaptive fiber based electronic skin for sensitive joint motion monitoring and tactile sensing. *Nano Energy* **2020**, *69*, No. 104429.
(43) Li, H.; Zhang, W.; Ding, Q.; Jin, X.; Ke, Q.; Li, Z.; Huang, C. Facile strategy for fabrication of flexible, breathable, and washable piezoelectric sensors via welding of nanofibers with multiwalled carbon nanotubes (MWCNTs). *ACS Appl. Mater. Interfaces* **2019**, *11*, 38023−38030.
(44) Abbasipour, M.; Khajavi, R.; Yousefi, A. A.; Yazdanshenas, M. E.; Razaghian, F.; Akbarzadeh, A. Improving piezoelectric and pyroelectric properties of electrospun PVDF nanofibers using nanofillers for energy harvesting application. *Polym. Adv. Technol.* **2019**, *30*, 279−291.
(45) Kim, M.; Kaliannagounder, V. K.; Unnithan, A. R.; Park, C. H.; Kim, C. S.; Sasikala, A. R. K. Development of In-Situ Poled Nanofiber Based Flexible Piezoelectric Nanogenerators for Self-Powered Motion Monitoring. *Appl. Sci.* **2020**, *10*, 3493.
(46) Zeyrek Ongun, M.; Oguzlar, S.; Doluel, E. C.; Kartal, U.; Yurddaskal, M. Enhancement of piezoelectric energy-harvesting capacity of electrospun β-PVDF nanogenerators by adding GO and rGO. *J. Mater. Sci.: Mater. Electron.* **2020**, *31*, 1960−1968.
(47) Abbasipour, M.; Khajavi, R.; Yousefi, A. A.; Yazdanshenas, M. E.; Razaghian, F. The piezoelectric response of electrospun PVDF nanofibers with graphene oxide, graphene, and halloysite nanofillers: a comparative study. *J. Mater. Sci.: Mater. Electron.* **2017**, *28*, 15942−15952.
(48) Fukushima, T.; Asaka, K.; Kosaka, A.; Aida, T. Fully plastic actuator through layer-by-layer casting with ionic-liquid-based bucky gel. *Angew. Chem., Int. Ed.* **2005**, *44*, 2410−2413.
(49) Soulestin, T.; Ladmiral, V.; Dos Santos, F. D.; Ameduri, B. Vinylidene fluoride-and trifluoroethylene-containing fluorinated electroactive copolymers. How does chemistry impact properties? *Prog. Polym. Sci.* **2017**, *72*, 16−60.
(50) Ma, Y.; Zhang, Y.; Cai, S.; Han, Z.; Liu, X.; Wang, F.; Feng, X. Flexible hybrid electronics for digital healthcare. *Adv. Mater.* **2020**, *32*, No. 1902062.

https://doi.org/10.1021/acsomega.2c02024
ACS Omega 2022, 7, 23521−23531